Food Research International 138 (2020) 109770

Contents lists available at ScienceDirect

Food Research International

journal homepage: www.elsevier.com/locate/foodres

Loading of lutein in egg-sphingomyelin vesicles as lipid carriers: Thermotropic phase behaviour, structure of sphingosome membranes and lutein crystals

Christelle Lopez [a,b,*], Cristelle Mériadec [c], Elisabeth David-Briand [a], Aurélien Dupont [d], Thomas Bizien [e], Franck Artzner [c], Alain Riaublanc [a], Marc Anton [a]

[a] INRAE, BIA, 44316 Nantes, France
[b] INRAE, STLO, 35000 Rennes, France
[c] IPR, UMR 6251, CNRS, University of Rennes 1, 35042 Rennes, France
[d] Univ Rennes, CNRS, Inserm, BIOSIT - UMS 3480, US_S 018, 35000 Rennes, France
[e] Synchrotron Soleil, L'Orme des Merisiers, Saint-Aubin BP48, 91192 Gif-sur-Yvette, France

ARTICLE INFO

Keywords:
Membrane bilayer
Sphingolipid
Encapsulation
Liposome
Carotenoid
Functional food

ABSTRACT

Lutein is a xanthophyll carotenoid provided exclusively by the diet, that has protective functions and beneficial effects on human health. Supplementation in lutein is necessary to reach the recommended daily dietary intake. However, the introduction of lutein into foods and beverages is a real challenge since this lipophilic nutrient has a poor aqueous solubility and a low bioavailability. In this study, we investigated the capacity of egg-sphingomyelin (ESM) vesicles called sphingosomes to solubilise lutein into the bilayers. The thermal and structural properties of ESM bilayers were examined in presence of various amounts of lutein by differential scanning calorimetry (DSC) and temperature-controlled X-ray diffraction (XRD), the structures of sphingosomes and lutein crystals were observed by microscopic techniques. ESM bilayers were in the fluid L_α phase above the phase transition temperature $T_m = 39.6$ °C and in the lamellar ripple $P_{\beta'}$ phase below T_m where ESM sphingosomes exhibited ondulations and were facetted. Lutein molecules were successfully incorporated into the ESM bilayers where they induced a structural disorganisation. For ESM/lutein 90/10 %mol (91.8/8.2 %wt; 89 mg lutein / g ESM), lutein partitioning occured with the formation of lutein crystals in the aqueous phase together with lutein-loaded ESM vesicles. This study highlighted the capacity of new lipid carriers such as egg-sphingosomes to solubilise lutein and opens perspectives for the formulation of effective lutein-fortified functionnal foods and beverages providing health benefits.

1. Introduction

Consumer's demand for more natural food products providing health benefits has increased over the years. A major challenge in the next years will therefore consist in producing healthy and sustainable foods with optimized nutritional quality. However, the incorporation of natural bioactive molecules into foods is often limited because of their low water solubility, chemical and physical instability, and low bioavailability. Further research studies on the developement of encapsulation systems able to improve the solubilisation of dietary bioactives, such as carotenoids, into aqueous food and beverage products are required.

Lutein, a prevalent natural xanthophyllic carotenoid, has been reported to provide several protective functions and to have beneficial effects on human health that are many related to its antioxidant activities. Lutein plays a role in the development of the visual and nervous systems of fetuses, the ocular health, protection against cardiovascular diseases (Buscemi et al., 2018; Gammone et al., 2015; Kim et al., 2011). Lutein is involved in the prevention of cataracts and age-related macular degeneration (AMD), which is a leading cause of irreversible blindness in people over 65 years old in industrialised countries (Aronow & Chew, 2014). Humans are unable to endogenously synthesize lutein carotenoid in the body, its presence in human tissues and tissue levels therefore entirely depend on dietary intake (Krinsky et al., 2003). Lutein can be found mainly in leafy greens (e.g. broccoli, spinach), in vegetables (e.g.

* Corresponding author at: INRAE, UR BIA, F-44316 Nantes, France.
E-mail address: christelle.lopez@inrae.fr (C. Lopez).

https://doi.org/10.1016/j.foodres.2020.109770
Received 2 May 2020; Received in revised form 30 July 2020; Accepted 30 September 2020
Available online 7 October 2020

corn), in Marigold flowers and in egg-yolk containing foods (Perry et al., 2009; Steiner et al., 2018; Zaheer, 2017). Despite the claimed benefits that lutein may bring to human health, the intake of natural dietary sources of this carotenoid is very low. For example, the average consumption of lutein is 0.48–0.64 mg per day in France; German and Canadian studies reported an average adult's lutein consumption of 1.9 mg and 1.4 mg per day, respectively, whereas Americans consume around 1–2 mg of lutein and zeaxanthin on average per day (Johnson et al., 2010; Li et al., 2020; Rasmussen & Johnson, 2013). However, the dose of lutein associated with a decreased risk of AMD is about 6–10 mg per day (Rasmussen & Johnson, 2013; Seddon et al., 1994). Epidemiological studies and intervention studies in humans provided evidence that the dietary intake of lutein may protect against AMD and prevent its progression (Eisenhauer et al., 2017; Ma et al., 2012; Wu et al., 2015). Studies showed that an increase in lutein dietary intake leads to increased serum levels (Handelman et al., 1999; Kelly et al., 2014; Thürmann et al., 2005). However, the bioavailability of lutein depends on many determinants and varies as a function of dietary sources (Desmarchelier & Borel, 2017). For example, Chung et al. (2004) showed in healthy men that lutein in egg exhibits a high bioavailability compared to other sources such as lutein, lutein ester supplements and spinach.

The prevalence of lutein in supplements is increasing (Mares, 2016). Furthermore, there is a need to develop effective diet-based strategies, such as food supplementation, to increase lutein intakes through lutein-fortified functional foods and then to overcome deficiencies in the human diet and to prevent eye diseases in both developing and developed countries (Rasmussen & Johnson, 2013). However, incorporation of lutein into aqueous foods and beverages is limited because of its chemical instability toward light, oxygen, and temperature, and its low water solubility inducing the formation of large crystals, leading to impaired antioxidant activities, poor absorption and low bioavailability. Recent research has shown that an appreciable amount of lutein (~60%) is not absorbed because of its low water-solubility and difficulty to be incorporated into mixed micelles or vesicles in the gastrointestinal tract (Kopec et al., 2017). The crystallization of bioactives that have high hydrophobicity and high melting points, such as lutein, needs to be overcomed. The solubilisation of these bioactive molecules in the aqueous phase of foods and in the gastrointestinal tract upon digestion seems therefore to be essential for their efficient absorption by the enterocytes and to improve their bioavailability. Recently, nanocrystal technology has been successfully investigated to improve oral bioavailability of lutein (Chang et al., 2018). Encapsulation is a promising method to achieve protection of lutein against physical damage, to preserve its chemical stability and to facilitate its incorporation into aqueous food and beverage products (Steiner et al., 2018). Strategies for the encapsulation of lutein in several delivery systems have been developed. Emulsions, simple or multiple, are the most common delivery systems for lutein (Steiner et al., 2018). The colloidal delivery systems are, for example, nanoparticles (Hu et al., 2012; da Silva Santos et al., 2019), microcapsules (Álvarez-Henao et al., 2018; Huang et al., 2019; Kuang et al., 2015), nanoemulsions (Murillo et al., 2016; Steiner et al., 2019) and lipid vesicles such as liposomes (Tan et al., 2013; Xia et al., 2012).

Lipid vesicles have, over the years, been considered as efficient carrier and delivery systems for bioactive molecules and drugs. They have been therefore widely used in various applications such as cosmetic, pharmaceutical and therapeutic applications, and are of increasing interest for food applications. An aqueous volume is enclosed by a single phospholipid bilayer (unilamellar vesicles or liposomes) or several concentric bilayer (multilamellar vesicles) membrane, in which the hydrophobic molecules are solubilised. Due to flexibility in size and lipid composition, different types of lipid vesicles have been developped and used. Most of lipid vesicles or liposomes designed for encapsulation are composed of glycerophospholipids. For food applications, lipid vesicles composed of glycerophospholipids such as soya lecithin, milk polar lipids or model systems such as dipalmitoyl-phosphatidylcholine, have been mainly investigated (Singh, 2006; Xia et al., 2012). Phospholipid suspensions composed of phosphatidylcholine enhanced the bioavailalbility of lutein and the accumulation into the retina of eyes (Shanmugam et al., 2011). The enhanced bioavailability of lutein from egg yolk reported by Chung et al. (2004) may be due to the presence of phosphatidylcholine and sphingolipids in egg yolk. To date, there is a relatively lack of published data for an other category of lipid vesicles composed of sphingolipids that are called sphingosomes (Swarnlata, 2011). Sphingosome encapsulated technology has first been used for pharmaceutical applications, where sphingosomes are administered in many ways including parenteral (e.g. intravenous, transdermal, inhalation) and enteral routes. Sphingomyelin (SM) molecules are the most abundant sphingolipids found in biological membranes, such as the apical membrane of the enterocytes, where they have structural functions and preferentially interact with cholesterol to form ordered domains called lipid rafts (Lopez et al., 2010; Simons & Ikonen, 1997). The chemical structure and physical properties of SM molecules are therefore prone to interactions with host molecules in the bilayer membranes. The natural sources of sphingolipids, mainly SM, are mammal milks, egg yolk, and brain. In addition to form sphingosomes as efficient lipid carrier systems, the importance of dietary sphingolipids in human nutrition and health has emerged in the last 20 years (Vesper et al., 1999).

In this work, we hypothesised that sphingosomes could be efficient lipid carriers to solubilise and protect lutein molecules in functional foods, to favour their uptake at the membrane of the enterocytes, and to improve their delivery to human body. Sphingosomes are composed of lipids that are similar to those found in biological membranes, there is therefore no restriction concerning their use in foods and beverages since they are biocompatible and accepted as safe. Egg-sphingomyelin (ESM) is a natural dietary sphingolipid found in egg yolk, composed of long saturated chains that could avoid the oxydation of lutein molecules as compared to natural unsaturated glycerophospholipids. The objectives of this study were therefore to examine the physical properties of lutein molecules (crystallization and melting properties) and to investigate the capacity of ESM bilayers to solubilise lutein molecules. The thermotropic phase behaviour and structural organization of lutein alone and ESM/lutein bilayers with various molar proportions have been examined as a function of temperature by using differential scanning calorimetry (DSC) and X-ray diffraction (XRD). The ESM/lutein samples were also observed using microscopy techniques.

2. Materials and methods

2.1. Materials

Lutein (purity > 99%; all-*trans*-lutein; MW: 568.87 g/mol) was purchased from Merck (Merck, Germany). Lutein molecules are terpenoid compounds with a long electron-rich conjugated polyene chain and two terminal hydroxyl groups located in ionone rings (Fig. 1).

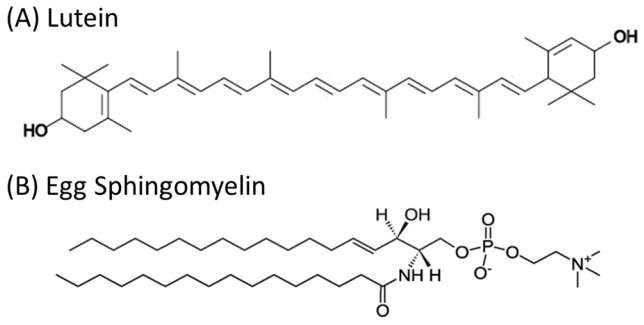

Fig. 1. Chemical structure of (**A**) lutein and (**B**) egg sphingomyelin.

Sphingomyelin from egg yolk (ESM; purity > 98%; MW: 703.04 g/mol) was purchased from Larodan (Larodan, Sweden). ESM is composed of a phosphocholine polar head group, a sphingosine backbone with an hydroxyl group, and an additional hydrocarbon chain attached *via* an amide linkage (Fig. 1). In ESM, this hydrocarbon chain is composed of long chain saturated fatty acids, mainly C16:0 (86%) and contains small amounts of C18:0 (6%) and C22:0 (3%). Purified water (Milli-Q Waters) was used for sample preparation.

2.2. Samples preparation

Samples were prepared by dissolving the appropriate amounts of ESM and lutein powders in chloroform/methanol (4/1 v/v) and mixing them from stock solutions in the desired proportions, denoted ESM/lutein molar ratios. The organic solvent was subsequently evaporated under a stream of dry nitrogen. The ESM sample was hydrated with water to reach the final concentration of 20 %wt ESM, for which ESM is fully hydrated. The ESM/lutein dried mixtures were hydrated with water to reach the final concentration of 20 %wt of ESM + lutein. The samples were expressed as the molar ratio between ESM and lutein. The ESM/lutein samples were as follows: 100/0 %mol (100 %wt ESM), 98/2 %mol (98.4/1.6 %wt), 95/5 %mol (95.9/4.1 %wt), 93/7 %mol (94.3/5.7 %wt), 90/10% mol(91.8/8.2 %wt), 88/12 %mol(90.1/9.9 %wt), 85/15 %mol (87.5/12.5 %wt), 80/20 %mol (83.2/16.8 %wt), 75/25 % mol (78.8/21.2 %wt), 70/30 %mol (74.3/25.7 %wt), 65/35 %mol (69.7/30.3 %wt), 60/40 %mol (65/35 %wt) and 50/50 %mol (55.3/44.7 %wt). The dispersions were heated at 60 °C, i.e. above the chain melting transition temperature T_m of ESM, and thoroughly mixed in a vortex stirrer in order to form large multilamellar vesicles and to ensure good sample homogeneity. Before DSC and XRD analysis, the samples were kept at 20 °C for equilibration during at least 24 h.

2.3. Differential scanning calorimetry (DSC)

DSC measurements were performed with a DSC Q1000 (TA Instruments, Newcastle, DE). Lutein powder or an aliquot of the ESM or ESM/lutein samples was loaded into DSC hermetically sealed aluminum pans (TA Instruments). An empty and hermetically sealed aluminum pan was used as reference. The calorimeter was calibrated with indium (ΔH_m = 28.41 J/g; Melting point = 156.66 °C). The DSC pans were introduced in the calorimeter at 20 °C. The thermotropic behavior of lutein powder was studied on heatings from 20 °C to 200 °C at 10 °C/min, and coolings from 200 °C to 20 °C at 10 °C/min. To study the thermotropic phase behavior of ESM bilayers and ESM/lutein samples, the samples were cooled down to 0 °C at 2 °C/min, heating scans were run at a rate of 2 °C/min from 0 °C to 80 °C and then cooling scans were recorded at 2 °C/min from 80 °C to 0 °C. Data analysis was performed using TA Universal Analysis program. The melting transition temperature (T_m) of ESM bilayers was taken at the peak maximum. Enthalpy changes of the transitions (ΔH_m) were obtained from the area under the peak and normalized by the ESM mass. To calculate the area under the peak, a baseline connecting the linear segments of the heat capacity curve between the initial and end point of the transition was substracted. The DSC experiments were performed at least in triplicate for each sample.

2.4. X-ray diffraction (XRD)

2.4.1. Temperature-controlled X-ray diffraction (XRD)

X-ray scattering experiments were performed on the home-made Guinier beamline at IPR (Rennes, France). A two-dimensional Pilatus detector with sample to detector distance of 232 mm allowed the recording of XRD patterns in the range 0.013–1.742 $Å^{-1}$, thus covering both the small and wide-angles regions of interest to characterize the lamellar structures and to identify the packing of the acyl chains, respectively. Diffraction patterns displayed series of concentric rings as a function of the radial scattering vector $q = 4\pi\sin(\theta)/\lambda$, where 2θ is the scattering angle and $\lambda = 1.541$ Å is the wavelength of the incident beam. The channel to scattering vector q calibration of the detector was carried out with silver behenate. Small volumes (around 10 μL) of samples containing ESM or ESM/lutein vesicles were loaded in thin quartz capillaries of 1.5 mm diameter (GLAS W. Muller, Berlin, Germany) and inserted in the set-up at a controlled temperature, i.e. $T = 20\,°C < T_{m\text{-}ESM}$ and $T = 55\,°C > T_{m\text{-}ESM}$. Each XRD pattern has been recorded for 900 sec. PeakFit software (Jandel Scientific, Germany) was used to determine the positions of the Bragg reflections.

2.4.2. Synchrotron-radiation XRD as a function of temperature (XRDT)

XRD measurements were performed as a function of temperature (XRDT) on the high brilliance SWING beam line at the Soleil synchrotron facility, with monochromator set at 15 KeV (David & Pérez, 2009). Using a EIGERX 4 M detector at 0.528 m from the sample, diffraction patterns were recorded for reciprocal spacing q varying between 0.024 and 2.8 $Å^{-1}$, that is, repetitive distances $d = 2\pi/q$ ranging from 262 to 2.2 Å. This q range covered both the small and wide-angles regions of interest to characterize the lamellar structures and to identify the packing of the acyl chains, respectively.1D XRD curves were obtained by circular averaging of the 2D images using the Foxtrot software. Samples of lutein powder, ESM and ESM/lutein vesicles were loaded into thin quartz capillaries of 1.5 mm diameter (GLAS W. Muller, Berlin, Germany). The capillaries were inserted into a THMS600 linkam oven (Linkam Scientific Instruments Ltd, Waterfield, UK) allowing temperature scan between −194 and 600 °C. This set-up allowed synchrotron-radiation XRDT. For lutein powder, the XRDT experiments were conducted on heating from 20 °C to 220 °C at 10 °C/min (1000 patterns; 0.4 sec exposure time and 0.8 sec gap time). For ESM and ESM/lutein (90/10 %mol) vesicles, XRDT experiments were conducted on heating from 20 °C to 60 °C at 2 °C/min (200 patterns; 2 sec exposure time and 4 sec gap time). The three-dimensional plots of XRD patterns as a function of temperature were displayed using R software (R Foundation for Statistical Computing, Vienna, Austria). PeakFit software (Jandel Scientific, Germany) was used to determine the positions of the Bragg reflections.

2.5. Microscopic observations

2.5.1. Cryo-EM

The samples containing multilamellar vesicles composed of ESM alone or with 5 %mol lutein were observed by cryo electron microscopy (cryo-EM). Vitrification of the samples was performed using an automatic plunge freezer (EM GP, Leica) under controlled humidity and temperature (Dubochet & McDowall, 1981). The samples were deposited to glow-discharged electron microscope grids followed by blotting and vitrification by rapid freezing into liquid ethane at −184 °C. Grids were transferred to a single-axis cryo-holder (model 626, Gatan) and were observed at −170 °C using a 200 kV electron microscope (Tecnai G2 T20 Sphera, FEI) equipped with a 4 k × 4 k CCD camera (model USC 4000, Gatan). Micrographs were acquired under low electron doses using the camera in binning mode 1 and at a nominal magnifications of 25 000×.

2.5.2. Confocal microscopy combined with DIC

The microstructural analysis was performed using an inverted microscope NIKON Eclipse-TE2000-C1si (NIKON, Champigny sur Marne, France) allowing confocal laser scanning microscopy (CLSM) and optical microscopy using differential interferential contrast (DIC) also called Nomarsky. Confocal experiments were performed using a He–Ne laser operating at 543 nm wavelength excitation (emission was detected between 565 and 615 nm). The observations were performed using x100 (NA 1.4) oil immersion objective. The bilayers of ESM vesicles were stained with the lipid-soluble Nile Red fluorescent dye (9-diethylamino-5H-benzoalpha-phenoxazine-5-one; Sigma–Aldrich, St Louis, USA),

After the labelling step, the samples were kept at room temperature

for at least 15 min before the microstructural analysis. Then, 5 μL of the samples stained with the fluorescent dye were deposited onto the glass and observed on the microscope. The microstructural analyses were performed at room temperature (e.g. 19 ± 1 °C). DIC was used to visualize both the lipid vesicles and the lutein crystals. DIC images were sometimes superimposed to the emission fluorescence recorded in the CLSM images. The two-dimensional images had a resolution of 512 × 512 pixels and the pixel scale values were converted into micrometers using a scaling factor.

3. Results and discussion

3.1. Powdered lutein crystals

Lutein molecules (Fig. 1) were organised as platelets of crystals in the commercial powder used for the experiments as shown Fig. 2-**A**. The physical state and melting behaviour of the powdered lutein crystals have been investigated by synchrotron radiation XRD as a function of temperature and by DSC. Fig. 2-**B** shows the time-resolved synchrotron radiation XRD patterns recorded as a function of temperature on heating of lutein powder from 20 °C to 220 °C. The strong diffraction peaks correspond to the crystalline state of lutein in the powder, as previously reported in literature (Hu et al., 2012). For temperatures above about 170 °C, the absence of diffraction peaks corresponds to an amorphous state of lutein molecules.

Fig. 2-**C** shows the thermotropic phase behaviour of lutein powder examined by DSC on subsequent heatings and coolings. On the first heating, the thermogram showed a broad exotherm and a sharp endotherm at $T_m = 168.4 \pm 2.8$ °C corresponding to the melting of the lutein crystals present in the powder. This result is in agreement with literature (Zhao et al., 2017). The T_m value recorded by DSC is in agreement with the phase transition characterised by synchrotron-radiation XRD in the same range of temperature (Fig. 2-**B**). On subsequent cooling, an exotherm was recorded at $T_c = 46.0 \pm 0.6$ °C. The second heating showed two successive endotherms at $T_{m1} = 58.8 \pm 0.1$ °C and $T_{m2} = 64.3 \pm 0.7$ °C. Differences in the melting temperatures measured after the first heating and the subsequent heatings may correspond to different molecular organisation of lutein molecules in the crystals and then to polymorphism in the solid state.

These XRD and DSC experiments demonstrated that lutein molecules

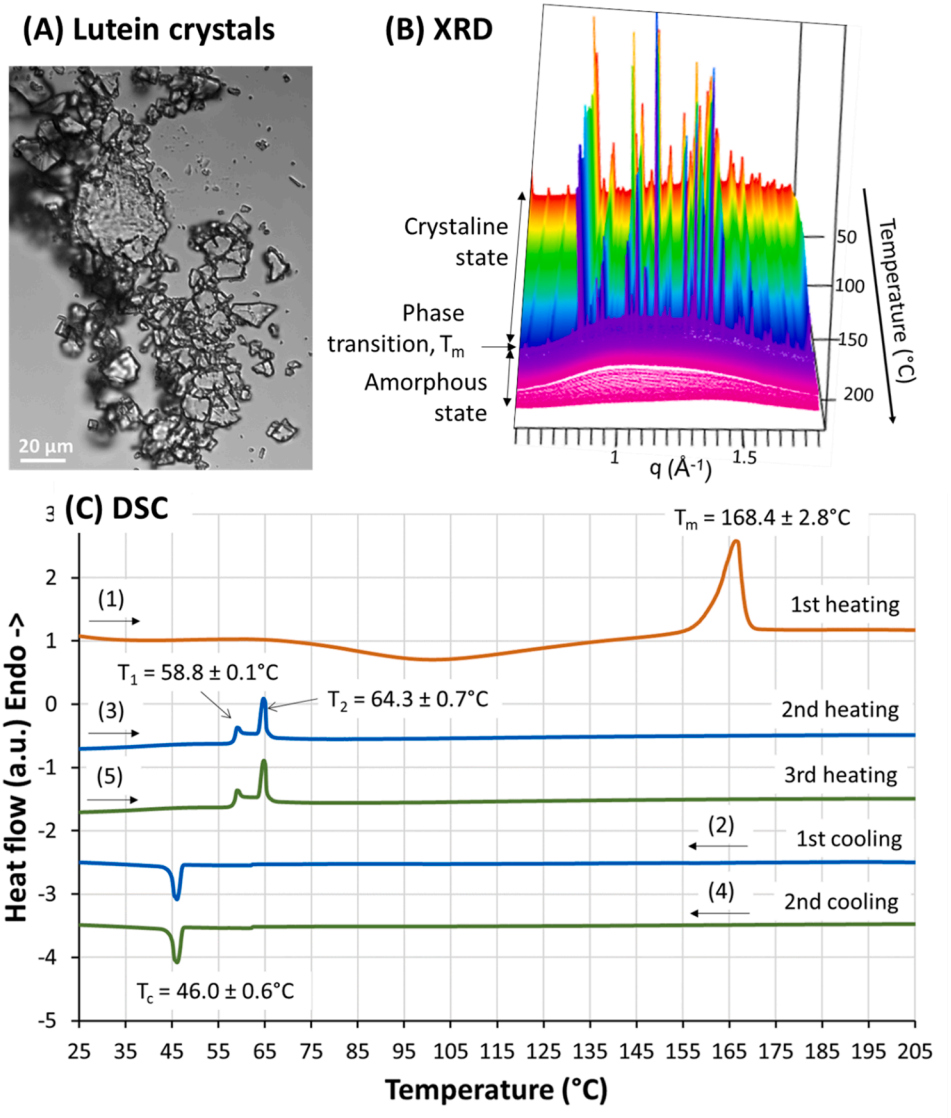

Fig. 2. Lutein powder: thermotropic and structural properties. **(A)** Microscopy image showing lutein crystals in the powder. **(B)** Synchrotron radiation X-ray diffraction (XRD) patterns of lutein powder recorded as a function of temperature on heating from 20 to 220 °C at 10 °C/min. **(C)** Thermal properties of lutein powder recorded by differential scanning calorimetry (DSC) on successive heatings and coolings at 10 °C/min.

are in a crystalline state up to 168 °C in the most stable crystalline state, and up to 58 °C in a least stable polymorphic state. This means that in all cases, lutein molecules are in a solid state at processing temperature in the food industry, at storage temperatures, and at human body temperature during digestion which is responsible for the low bioavailability of lutein.

3.2. Egg-sphingomyelin multilamellar vesicles: Thermotropic phase behaviour and structural properties

Thermograms of fully hydrated and equilibrated ESM multilamellar vesicles, i.e. sphingosomes, were recorded on heating (Fig. 3). Multilamellar vesicles of ESM exhibited a single sharp endotherm. The phase transition temperature was T_m = 39.6 ± 0.1 °C. The calorimetric enthalpy of melting was ΔH_m = 6.8 ± 0.1 kcal/mol. These DSC results obtained for ESM multilamellar vesicles in water agree well with those of previous studies (Chemin et al., 2008; Mannock et al., 2003; Ramstedt & Slotte, 1999). The thermograms recorded on heating were reversible and reproducible upon cooling and immediate reheating (Fig. 3). The sharpness of the endotherm indicated a high packing of ESM molecules in the bilayers and a highly cooperative phase transition. The sharp endotherm arises from the fact that ESM contains a high proportion of C16:0 acyl chains (>80% by weight of the total fatty acyl chains), and must be due to the chain melting phase transtition of N-palmitoyl SM. For comparison, fully hydrated multilamellar vesicles composed of the synthetic C16:0-SM molecules (N-palmitoyl-D-*erythro*-sphingosylphosphorylcholine; d18:1/16:0; purity > 99%), exhibited a sharp phase transition at 41 °C upon heating by DSC (Et-Thakafy et al., 2018). The highly cooperative phase transition exhibited by ESM is unusual as compared to other natural SM that exhibit more complex and broad endotherms due to the presence of several SM molecular species and polymorphism, for example milk SM (Lopez et al., 2018).

XRD patterns of ESM multilamellar vesicles were recorded at 20 °C (i.e. below T_m), and 55 °C (i.e. above T_m) to identify the structural

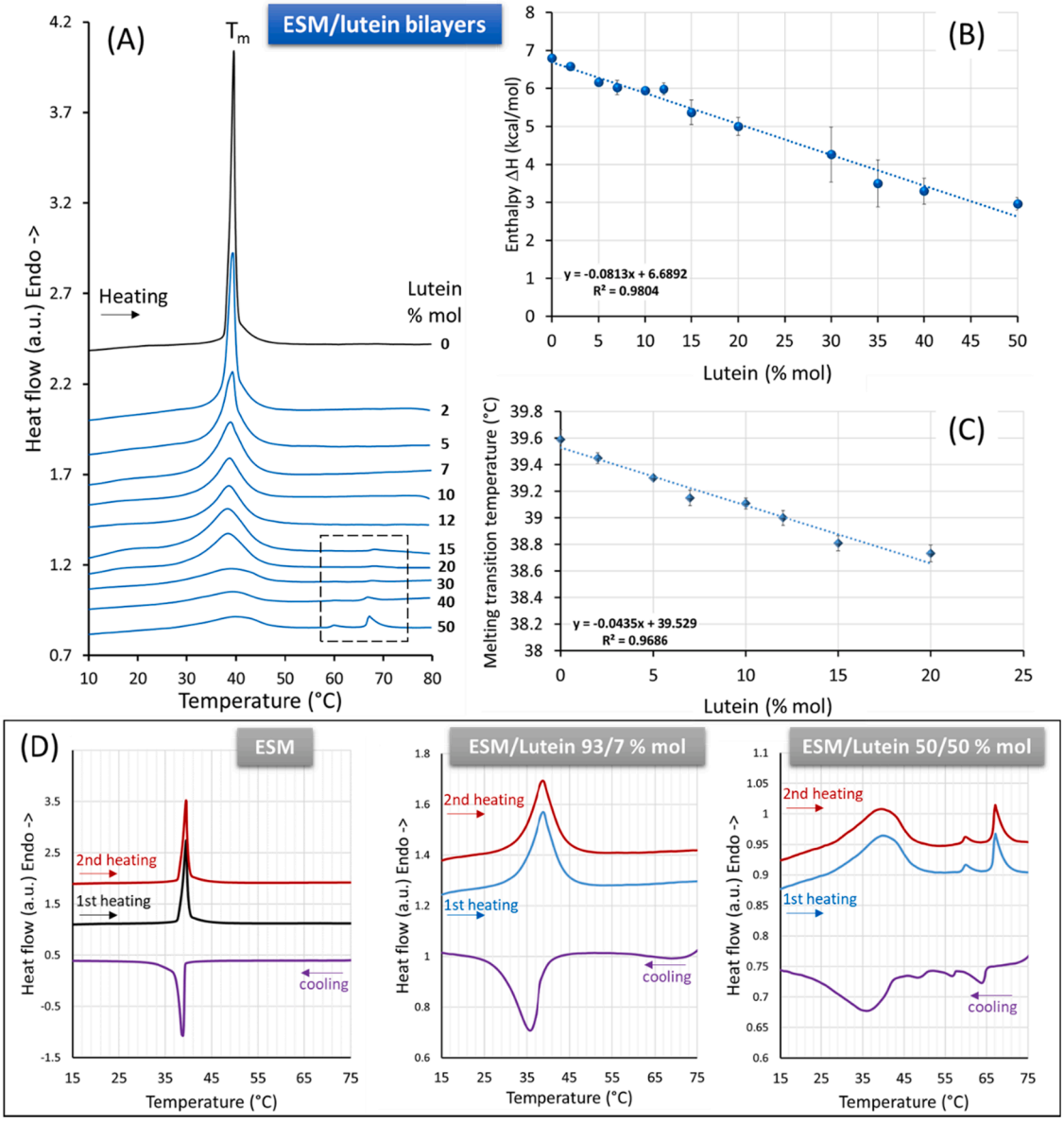

Fig. 3. Effect of lutein on the thermotropic phase behavior of egg sphingomyelin (ESM) bilayers revealed using differential scanning calorimetry (DSC). **(A)** Thermograms recorded on heating at 2 °C/min of ESM/lutein samples, with the molar fraction of lutein indicated in the figure. **(B)** Melting enthalpy as a function of lutein concentration. **(C)** Melting transition temperature T_m as a function of lutein concentration. **(D)** Thermograms recorded on heating, cooling and immediate reheating at 2 °C/min of fully hydrated ESM/lutein bilayers with various molar ratios indicated in the figures.

parameters of the bilayers and the organisation of ESM molecules (Fig. 4).

At 20 °C, the XRD pattern recorded at small angles exhibited several peaks that could be indexed on a two-dimensional lattice (Fig. 4**-A and B**). The broad peaks corresponded to the first (01), second (02), third (03) and fouth (04) order of a lamellar structure. The lamellar repeat distance deduced from the (01) reflection was d = 66.4 Å (q = 0.0947 $Å^{-1}$). A weak peak at very small angles ((10) peak) was observed at q = 0.0458 $Å^{-1}$ and yielded the ripple length of the phase (Fig. 4**-A**). The broad first-order peak of the lamellar structure was composed of two overlapped lines, assigned to the (01) reflection and (11) reflection of the ripple phase. The ripple reflections were rather diffuse, probably due to a weak in-plane correlation of the bilayers. The accurate analysis of the reciprocal lattice vector q_{hk} permitted the determination of the structural parameters of the ripple phase. The small-angle XRD Bragg peaks with Miller indices (h,k) were indexed to a two-dimensional unit cell, h indexing the bilayer packing repeat distance d and k indexing the ripple wavelength λ_{ripple}. The oblique angle γ for the unit cell was also determined. The structural parameters of the ripple phase formed by ESM bilayers were λ_{ripple} = 139.8 Å, d = 65.6 Å, γ = 94°. At wide angles (Fig. 4**-C**), the single peak observed at the d-spacing 4.16 Å (q = 1.51 $Å^{-1}$) was typical of hexagonally packed extended hydrocarbon chains in the gel phase. The XRD patterns recorded at both small and wide angles for ESM multilamellar vesicles at 20 °C were assigned to the formation of a gel ripple phase $P_{\beta'}$. This $P_{\beta'}$ phase was first described by (Tardieu et al., 1973) and consist of regularly spaced bilayers distorted by a periodic ripple. Ripples are generally ascribed to a relative sliding of neighboring chains along their axes, with all chains tilted by the same average angle along the direction of rippling. Observation of a modulated phase in ESM bilayers suggests that the hydrocarbon chains were tilted at low temperature. The reason for ESM chain tilt is probably that the polar head group has a larger area in the plane of the bilayer than the hydrocarbon chains. Consequently, the hydrocarbon chains tilt to maximize their van der Waals interactions and to minimize headgroups

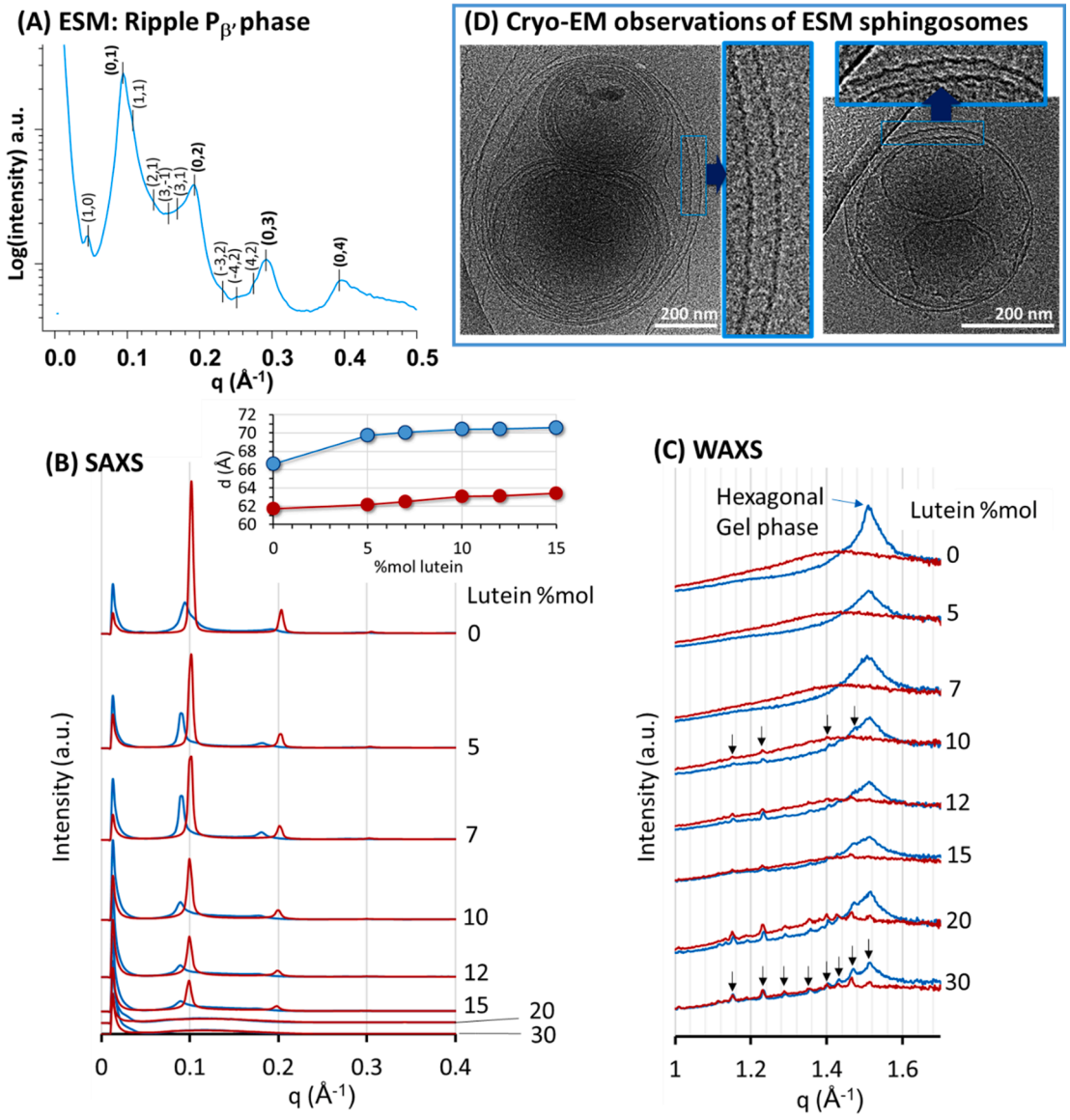

Fig. 4. Structure of sphingosomes composed of egg sphingomyelin (ESM) and lutein. **(A)** X-ray diffraction (XRD) pattern recorded at small angles for ESM sphingosomes at 20 °C, with indexation. Structural behavior of ESM bilayers containing various concentrations of lutein examined at 20 °C (blue colour) and 55 °C (red colour) using XRD **(B)** at small angles (SAXS) and **(C)** at wide angles (WAXS); arrows indicate XRD signal from lutein crystals. Insert of (**B**): changes in the distance of the first order small-angle XRD peak as a function of lutein amount, determined at 20 °C and 55 °C. **(D)** Cryo electron microscopy images showing the ripples in ESM bilayers and the facets of sphingosomes. Abbreviation: q = scattering vector. (For interpretation of the references to colour in this figure legend, the reader is referred to the web version of this article.)

crowding (McIntosh, 1980). The formation of such $P_{\beta'}$ phase by ESM fully hydrated multilamellar vesicles has been previously described by (Chemin et al., 2008) using XRD as a function of temperature. Cryo electron microscopy (cryo-EM) observations allowed the visualization of ESM sphingosomes of varying size and structural complexity, i.e. multilamellar vesicles with regularly spaced bilayers and oligo-vesicular vesicles (Fig. 4-**D**). Cryo-EM images showed that the membrane of sphingosomes was distorted by a periodic ripple and exhibited ondulations confirming information provided by XRD experiments. Furthermore, ESM lipid vesicles exhibited an inhomogeneous curvature with flat facets. This facetted shape of ESM sphingosomes is a significant feature corresponding to the disruption of the gel packing by curvature, as already reported for DPPC vesicles (Stelter & Keyes, 2019). CLSM experiments performed at 20 °C showed that large ESM sphingosomes in the $P_{\beta'}$ phase exhibited a multilamellar organisation, with distorsions in the membrane and facets (Fig. 5).

At 55 °C, i.e. above the melting temperature T_m of ESM vesicles as characterised by DSC, XRD patterns recorded at small angles exhibited sharp and intense peaks, corresponding to the first orders of diffraction of a lamellar phase with a repeat distance d = 62 Å (01; q = 0.10146 $Å^{-1}$) (Fig. 4-**B**). The XRD patterns recorded at wide angles showed a bump of diffusion corresponding to the ESM acyl chains in the melted state (Fig. 4-**C**). Above T_m, ESM bilayers were in a lamellar liquid-crystalline L_α phase and the ripple $P_{\beta'}$ phase was no longer formed. The shift of the d-spacing towards lower values above T_m and the disappearance of the XRD peak at wide angles corresponded to the gel $P_{\beta'}$ to L_α phase transition that occured on heating of ESM fully hydrated multilamellar vesicles.

XRD patterns of ESM multilamellar vesicles were also recorded as a function of temperature thanks to the high flux of Soleil synchrotron (Fig. 6-**A**). The 3D plots of the SAXS and WAXS patterns recorded on heating show the $P_{\beta'}$ to L_α phase transition of ESM bilayers that occured between 35 and 45 °C. This phase transition correlated well with the endotherm recorded by DSC (Fig. 3).

3.3. *Influence of the incorporation of lutein in ESM bilayers and formation of lutein crystals*

3.3.1. *Thermotropic phase behaviour*

The impact of the addition of lutein on the thermal behavior of ESM bilayers was examined by DSC. Indeed, the degree of ordering of the ESM molecules in the sphingosome bilayers can be associated with the enthalpy values recorded in the melting events. On addition of various molar percentages of lutein in the ESM/lutein samples, the endothems recorded on heating evolved, demonstrating the incorporation of lutein molecules in the ESM bilayers (Fig. 3). Increasing lutein concentration in ESM bilayers induced i) a broadening of the endotherm interpreted as a decrease in the cooperativity of the ESM acyl chains upon phase transition, ii) a decrease of the melting enthalpy ΔH_m (Fig. 3-**B**) and iii) a small shift in the melting temperature T_m towards lower values (Fig. 3-**C**), compared to ESM bilayers alone. The decreases in the melting enthalpy ΔH_m and in the ordered to fluid L_α phase transition temperature T_m of ESM bilayers were assigned to a disorganisation of ESM in the gel phase due to a decrease in the hydrophobic interactions between the host ESM molecules when the lutein molecules integrated the bilayers. Whatever the lutein concentration, the thermograms recorded on heating and corresponding to the gel - L_α phase transition of ESM bilayers were reversible and reproducible upon cooling and immediate reheating (Fig. 3). This means that the phase transition of ESM bilayers did not induce a discharge of lutein molecules outside the sphingosomes together with structural reorganisations in the membranes. The thermotropic phase behavior of ESM bilayers in presence of lutein was different from the behavior observed in presence of cholesterol, where ΔH_m decrease with increasing cholesterol concentration until its disappearance for 40–50 mol% cholesterol that corresponds to the completion of the liquid-ordered L_o phase (Chemin et al., 2008). This means that the structure of the loaded molecules plays a major role in the organization of the host lipid bilayers.

For lutein content above 12 %mol in the ESM/lutein binary systems (90.1/9.9 %wt), endothermic events were recorded between 58 and 70 °C (Fig. 3). According to the thermotropic phase bilayer of the lutein powder (Fig. 2-**C**), they were attributed to the melting of lutein crystals

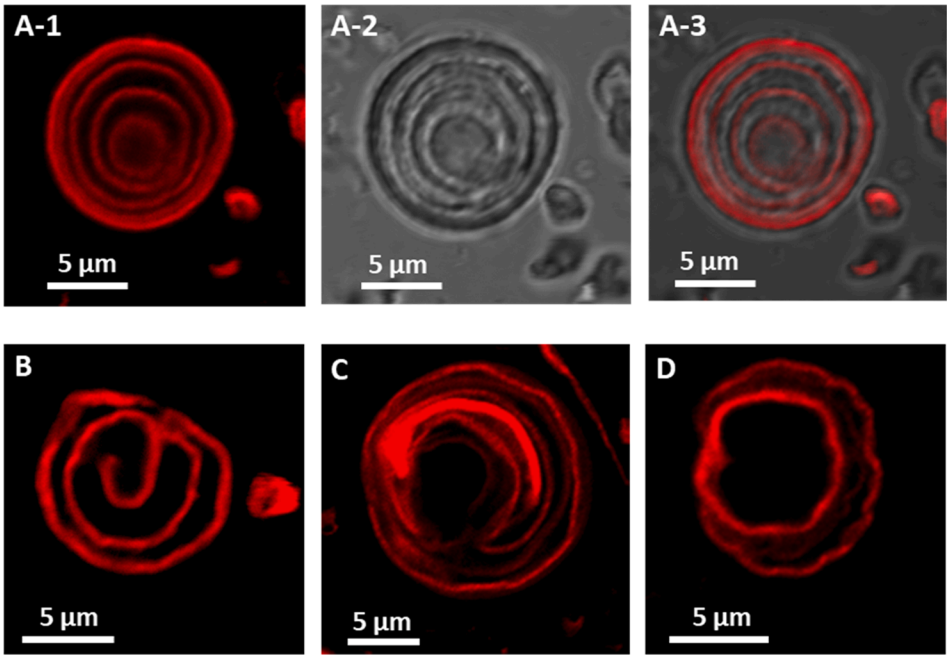

Fig. 5. Microscopy images showing egg sphingomyelin (ESM) sphingosomes. Confocal laser scanning microscopy (CLSM) with the Nile Red fluorescent dye to label the hydrophobic part of the ESM sphingosome bilayers (red colour). DIC images are in grey levels. Fig A-3 is the superimposition of CLSM (A-1) and DIC (A-2) images. (For interpretation of the references to colour in this figure legend, the reader is referred to the web version of this article.)

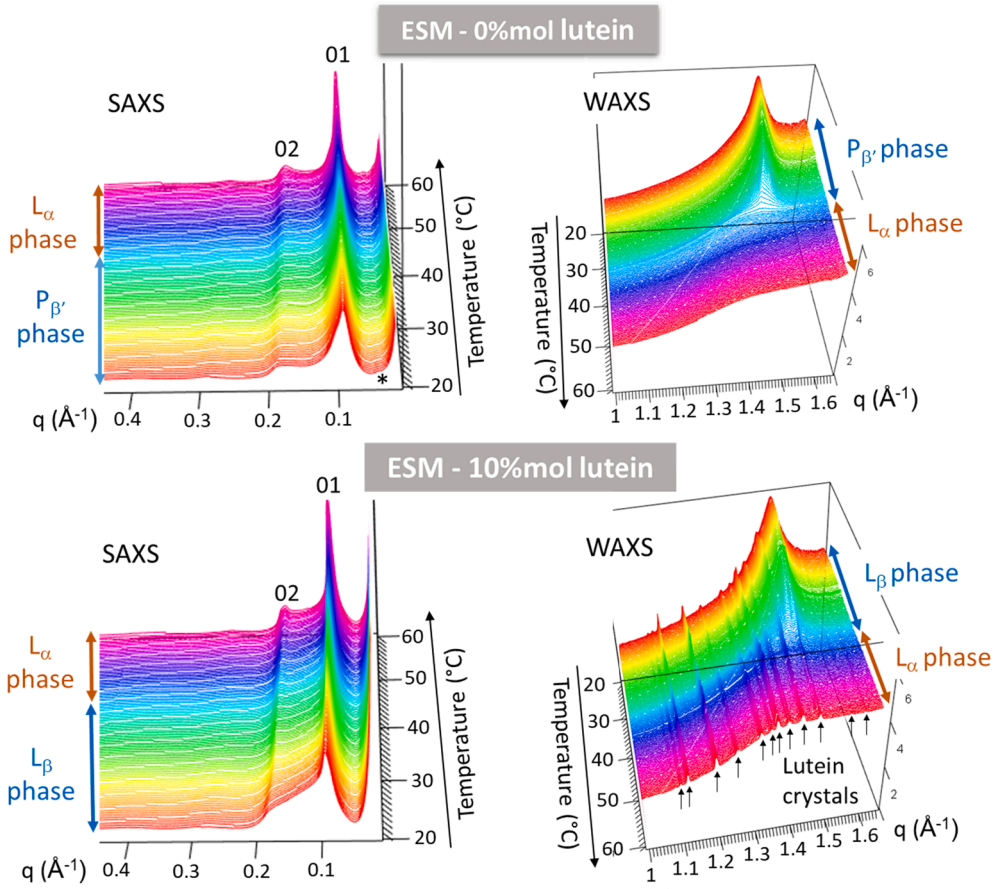

Fig. 6. Thermotropic phase behaviour of fully hydrated egg sphingomyelin (ESM) bilayers alone or ESM/lutein (90/10 %mol) samples examined using synchrotron radiation X-ray diffraction as a function of temperature (SR-XRDT) on heating at 2 °C/min. Three-dimensional plots of the XRD patterns recorded as a function of temperature at small (SAXS, left) and wide (WAXS, right) angles. q = scattering vector.

in the aqueous phase.

3.3.2. *Structural properties of ESM/lutein samples*

The structure of the ESM/lutein samples was investigated at different scale levels to fully identify the objects formed. The organisation of sphingosome membranes was characterised by XRD. At a higher scale level, the sphingosomes and lutein crystals were observed by microscopic techniques, i.e. confocal microscopy combined with DIC.

XRD patterns of ESM/lutein samples were recorded at 20 °C and at 55 °C, i.e. below and above the melting temperature of ESM bilayers determined by DSC, for increasing lutein concentrations (Fig. 4). Changes in the XRD patterns showed that the presence of lutein in the ESM/lutein binary systems affected the structural organisation of the ESM bilayers both below and above the phase transition temperature. At 20 °C, small angle XRD patterns showed reflections that indexed as orders of a lamellar repeat period. The d-spacing of ESM bilayers, corresponding to the membrane ESM bilayer unit cell periodicity including surface hydration, was increased in presence of lutein as compared to ESM bilayers alone (Fig. 4**-B insert**), which can be due to ESM chains becoming more perpendicular to the bilayer plane. Upon addition of 5 % mol lutein in the ESM/lutein samples (95.9/4.1 %wt) and more, the peak characteristic of the gel ripple $P_{\beta'}$ phase was absent. Wide-angle XRD patterns showed a single peak at 4.16 Å (1.51 $Å^{-1}$) that corresponded to a gel phase. The ripple phase was therefore converted into an untilted, L_{β}-like gel phase upon lutein incorporation. These XRD results revealed the presence of lutein molecules within the ESM bilayers. For 10 %mol lutein in the ESM/lutein samples (91.8/8.2 %wt), wide-angle XRD patterns showed a broad peak at 1.51 $Å^{-1}$ characteristic of the gel phase of ESM bilayers below T_m. Furthermore, small XRD peaks were recorded at 1.1548 $Å^{-1}$, 1.2331 $Å^{-1}$, 1.4062 $Å^{-1}$ and 1.4749 $Å^{-1}$. These XRD peaks recorded for 10 %mol lutein in the ESM/lutein samples were attributed to the formation of lutein crystals, in agreement with previous XRD examination of lutein crystals (Fig. 2) (Huang et al., 2019; Zhao et al., 2017). Above T_m, the acyl chains of ESM bilayers melted as indicated by a bump of diffusion at wide angles, while lutein crystals remained in their crystalline state as revealed by their XRD signature. Fig. 6 shows the synchrotron-radiation XRD patterns recorded as function of temperature on heating of the ESM/lutein 90/10 %mol sample (91.8/8.2 %wt). On heating, the L_{β} to L_{α} phase transition of ESM bilayers occured while the lutein crystals remained unaffected by the increase in temperature.

For lutein amount above 15 %mol (ESM/lutein 87.5/12.5 %wt), the lamellar organisation of the ESM molecules was no longer detected below and above the phase transition temperature (Fig. 4**-B**). The WAXS peak at 4.16 Å was consistent with hexagonal packing of extended chains in the gel phase below T_m wheareas ESM chains were melted above T_m. These XRD results revealed bilayers irregular and weakly correlated with a high disorder in the longitudinal stacking of ESM bilayers due to the presence of lutein molecules. Even above T_m where the melted chains have high mobility and cross-sectional area, the presence of lutein molecules leads to disordered bilayer stacking. At high lutein concentration in the ESM bilayer, partial aggregation of lutein molecules could occur within the lipid phase, as previously reported (Sujak et al., 2000).

Microscopy images showed the multilamellar sphingosomes formed in presence of lutein and confirmed the formation of long lutein crystals in the aqueous phase of the samples for lutein content above 10 %mol in the ESM/lutein samples (91.8/8.2 %wt) (Fig. 7). This means that a

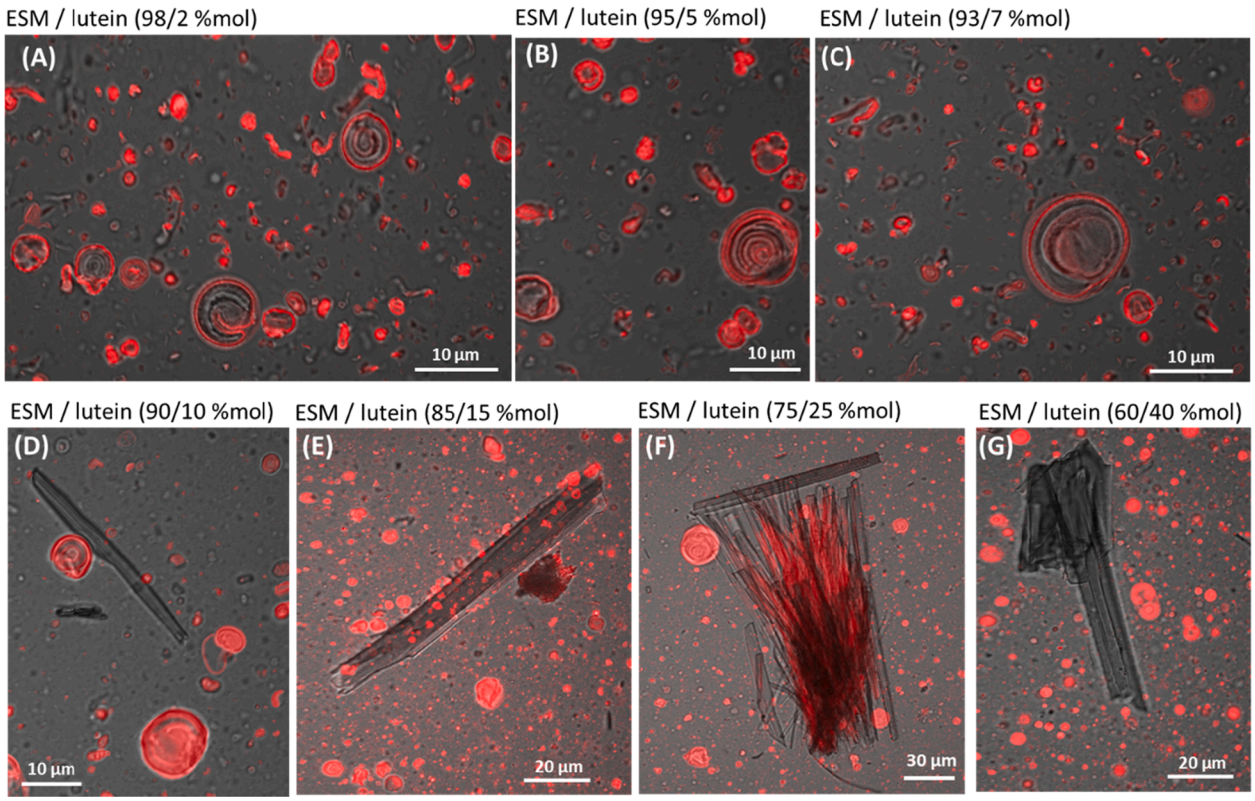

Fig. 7. Microscopy images showing egg sphingomyelin (ESM) sphingosomes loaded with lutein and lutein crystals. The images correspond to various proportions of lutein in the ESM/lutein samples as indicated in the figure. Confocal laser scanning microscopy (CLSM) with the Nile Red fluorescent dye to label the hydrophobic part of the ESM sphingosome bilayers (red colour). Combination with DIC images (grey colour). The images show the superimposition of CLSM and DIC images. (For interpretation of the references to colour in this figure legend, the reader is referred to the web version of this article.)

partitioning of lutein molecules occured. Lutein molecules were solubilised in the ESM bilayers of sphinposomes and lutein crystals were formed in the aqueous phase.

3.3.3. *Solubility of lutein in sphingosomes: Upon new lipid carriers for food applications*

In this study, we showed that ESM bilayers can be loaded with lutein molecules (Fig. 8). Lutein molecules act as spacers and interact with ESM molecules inside the ESM bilayer. We also found that lutein molecules form crystals in the aqueous phase for lutein content above 10 % mol in the ESM/lutein binary system (91.8/8.2 %wt; 89 mg lutein / g ESM).

For lutein content below 89 mg lutein / g ESM, egg-sphingosomes can therefore be considered as efficient lipid carriers without any

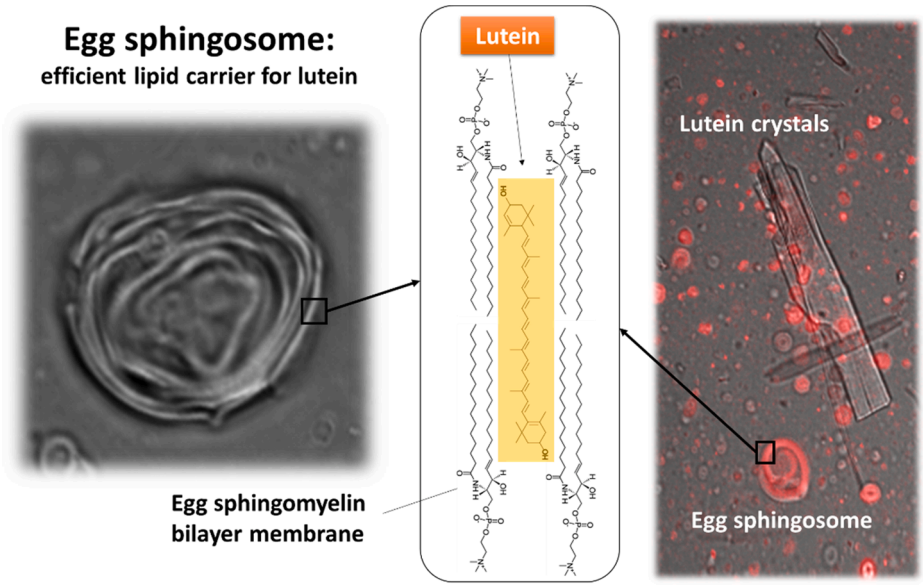

Fig. 8. Illustration of the insertion of lutein within a egg-sphingomyelin bilayer together with microscopy images showing lutein-loaded sphingosomes and lutein crystals.

formation of lutein crystals in the aqueous phase. To provide the dose of lutein associated with a decreased risk of AMD, i.e. 6–10 mg/day (Rasmussen & Johnson, 2013; Seddon et al., 1994), the preparation of fully hydrated sphingosomes with a formulation of 10 mg lutein with 113 mg ESM could be used.

The organisation of lutein molecules within the ESM bilayers and the interactions between lutein and ESM molecules need further discussions.

All carotenoid molecules present an hydrophobic character. Nevertheless, the terminal hydroxyl groups of the xanthophylls, such as lutein, provide a certain polar character, a potential interfacial activity as well as the ability to bind with other molecules, through intermolecular hydrogen bonds. Structural features such as size, shape, and polarity are essential determinants of the ability of a carotenoid to fit correctly into its molecular environment to allow it to function. The insertion of lutein molecules within ESM bilayers was permitted thanks to the chemical structure of lutein, i.e. presence of terminal hydroxyl groups at the end of the apolar all-*trans* chain (Fig. 1). XRD and DSC experiments performed in this study showed that the addition of lutein molecules prevented the formation of the ripple $P_{\beta'}$ phase and altered the structural organisation of ESM molecules in the bilayers both in the gel and in the fluid states (Fig. 4). We observed an increase in the ESM bilayer thickness as a function of lutein addition (Fig. 4), both in the gel and the L_{α} sate, which is in favour of a vertical intercalation of lutein molecules in the ESM bilayers (Fig. 8). According to their size, lutein molecules may match the double layer of ESM. In this organization, the polar part of the lutein molecules may be localized close to the hydrophilic group of ESM, while the hydrophobic part is oriented parallel to the hydrocarbon chains of ESM molecules. The interactions between lutein molecules and ESM bilayers may involve various forces. Each hydroxyl group of lutein can interact with the ESM polar headgroups (particularly the amide portion of ESM) in the opposite leaflet with H-bonds. Furthermore, short-distance van der Waals interactions can occur between saturated long chains of ESM which are dominated by C16:0 chains and the hydrophobic all-*trans* chain of lutein. Above T_m, the melted acyl chains of ESM bilayers have a greater flexibility and may impose a lower resistance to the lutein motion within the bilayer as compared to the gel phase. Also, the hydrophobic and van der Waals interactions between the melted acyl chains of ESM and the relatively rigid chain of lutein may be reduced. These interactions between lutein molecules and ESM organised as bilayers are the molecular origin of the solubility of lutein in sphingosomes. Our interpretation is in agreement with recent studies performed using a computational approach reporting that the orientation of lutein in a bilayer membrane is predominantly vertical (Makuch et al., 2019). Furthermore, using experimental and computational approaches, (Grudzinski et al., 2017) found that lutein molecules in dimyristoylphosphatidylcholine (DMPC with acyl chains C14:0) bilayers are oriented vertically with a 40 deg average tilt angle relative to the membrane normal. This tilt angle results from hydrophobic mismatch between the membrane thickness and the distance between the terminal hydroxyl groups of the lutein molecules. Experimental studies also predicted an horizontal orientation in which both hydroxyl groups interact with lipid headgroups in the same bilayer leaflet (Pasenkiewicz-Gierula et al., 2012; Sujak et al., 2000). Possibilities of reorientation of lutein molecules in the phospholipid bilayer, from horizontal to vertical and *vice versa*, have also been reported.

4. Conclusion

Lutein molecules remain in a crystalline state with a melting temperature above the human physiological temperature and would not be bioavailable in the human gastro-intestinal tract following digestion. It is therefore necessary to find solutions able to solubilise lutein molecules for food applications. In this study, we showed that egg sphingosomes are able to solubilise lutein molecules within their bilayer membrane, both in the gel and fluid states. However, above a lutein content of 10 % mol in the ESM/lutein samples (91.8/8.2 %wt; 89 mg lutein / g ESM), a partitioning of lutein molecules between the bilayers of ESM sphingosomes and the aqueous phase occurs. Lutein molecules forming crystals in the aqueous phase are no further integrated in the ESM sphingosomes and therefore will not be bioavailable. Furthermore, the lutein crystals in the form of anisotrope platelets of several μm long may play *in vivo* an irritative or deleterous abrasive role in the gastro-intestinal tract that should be further investigated. We showed for the first time in this study that egg sphingosomes loaded with lutein, with a formulation of 80 mg lutein / g ESM, could be interesting lipid carriers. Further *in vitro* and *in vivo* assays should be carried out to address the effectiveness of ESM sphingosomes in fortified foods in order to decrease the risk of AMD.

CRediT authorship contribution statement

Christelle Lopez: Conceptualization, Supervision, Writing - review & editing. **Cristelle Mériadec:** Investigation. **Elisabeth David-Briand:** Investigation. **Aurélien Dupont:** Investigation. **Thomas Bizien:** Investigation. **Franck Artzner:** Conceptualization, Formal analysis, Writing. **Alain Riaublanc:** Conceptualization, Writing. **Marc Anton:** Conceptualization, Writing.

Declaration of Competing Interest

The authors declare no conflict of interest

Acknowledgements

The authors thank synchrotron Soleil for allocating beam time on the SWING beamline as well as all the members of the Scientific Users Committee of INRAE. C. Lopez thanks Bérénice Houinsou-Houssou (INRAE, BIA, ISD) and Virginie Lollier (INRAE, BIA, BIBS) for their help in writing the programs with R software.

References

Álvarez-Henao, M. V., Saavedra, N., Medina, S., Jiménez Cartagena, C., Alzate, L. M., & Londoño-Londoño, J. (2018). Microencapsulation of lutein by spray-drying: Characterization and stability analyses to promote its use as a functional ingredient. *Food Chemistry, 256*, 181–187.

Aronow, M. E., & Chew, E. Y. (2014). AREDS2: Perspectives, recommendations, and unanswered questions. *Current Opinion in Ophthalmology, 25*, 186–190.

Buscemi, S., Corleo, D., Di Pace, F., Petroni, M. L., Satriano, A., & Marchesini, G. (2018). The effect of lutein on eye and extra-eye health. *Nutrients, 10*.

Chang, D., Ma, Y., Cao, G., Wang, J., Zhang, X., Feng, J., & Wang, W. (2018). Improved oral bioavailability for lutein by nanocrystal technology: Formulation development, in vitro and in vivo evaluation. *Artificial Cells, Nanomedicine, and Biotechnology, 46* (5), 1018–1024.

Chemin, C., Bourgaux, C., Péan, J.-M., Pabst, G., Wüthrich, P., Couvreur, P., & Ollivon, M. (2008). Consequences of ions and pH on the supramolecular organization of sphingomyelin and sphingomyelin/cholesterol bilayers. *Chemistry and Physics of Lipids, 153*(2), 119–129.

Chung, H.-Y., Rasmussen, H. M., & Johnson, E. J. (2004). Lutein bioavailability is higher from lutein-enriched eggs than from supplements and Spinach in men. *Journal of Nutrition, 134*(8), 1887–1893.

David, G., & Pérez, J. (2009). Combined sampler robot and high-performance liquid chromatography: A fully automated system for biological small-angle X-ray scattering experiments at the Synchrotron SOLEIL SWING beamline. *Journal of Applied Crystallography, 42*(5), 892–900.

Desmarchelier, C., & Borel, P. (2017). Overview of carotenoid bioavailability determinants: From dietary factors to host genetic variations. *Trends in Food Science & Technology, 69*, 270–280.

Dubochet, J., & McDowall, A. W. (1981). Vitrification of pure water for electron microscopy. *Journal of Microscopy, 124*, 3–4.

Eisenhauer, B., Natoli, S., Liew, G., & Flood, V. M. (2017). Lutein and Zeaxanthin—Food sources, bioavailability and dietary variety in age-related macular degeneration protection. *Nutrients, 9*.

Et-Thakafy, O., Delorme, N., Guyomarc'h, F., & Lopez, C. (2018). Mechanical properties of milk sphingomyelin bilayer membranes in the gel phase: Effects of naturally complex heterogeneity, saturation and acyl chain length investigated on liposomes using AFM. *Chemistry and Physics of Lipids, 210*, 47–59.

Gammone, M. A., Riccioni, G., & D'Orazio, N. (2015). Carotenoids: potential allies of cardiovascular health? *Food & Nutrition Research, 59*.

Grudzinski, W., Nierzwicki, L., Welc, R., Reszczynska, E., Luchowski, R., Czub, J., & Gruszecki, W. I. (2017). Localization and orientation of xanthophylls in a lipid bilayer. *Scientific Reports, 7*(1), 1–10.
Handelman, G. J., Nightingale, Z. D., Lichtenstein, A. H., Schaefer, E. J., & Blumberg, J. B. (1999). Lutein and zeaxanthin concentrations in plasma after dietary supplementation with egg yolk. *The American Journal of Clinical Nutrition, 70*, 247–251.
Hu, D., Lin, C., Liu, L., Li, S., & Zhao, Y. (2012). Preparation, characterization, and in vitro release investigation of lutein/zein nanoparticles via solution enhanced dispersion by supercritical fluids. *Journal of Food Engineering, 109*(3), 545–552.
Huang, J., Bai, F., Wu, Y., Ye, Q., Liang, D., Shi, C., & Zhang, X. (2019). Development and evaluation of lutein-loaded alginate microspheres with improved stability and antioxidant. *Journal of the Science of Food and Agriculture, 99*(11), 5195–5201.
Johnson, E. J., Maras, J. E., Rasmussen, H. M., & Tucker, K. L. (2010). Intake of Lutein and Zeaxanthin Differ with Age, Sex, and Ethnicity. *Journal of the American Dietetic Association, 110*(9), 1357–1362.
Kelly, E. R., Plat, J., Haenen, G. R. M. M., Kijlstra, A., & Berendschot, T. T. J. M. (2014). The effect of modified eggs and an egg-yolk based beverage on serum lutein and zeaxanthin concentrations and macular pigment optical density: Results from a randomized trial. *PLOS One, 9*, e92659.
Kim, J. E., Leite, J. O., deOgburn, R., Smyth, J. A., Clark, R. M., & Fernandez, M. L. (2011). A lutein-enriched diet prevents cholesterol accumulation and decreases oxidized LDL and inflammatory cytokines in the aorta of guinea pigs. *Journal of Nutrition, 141*, 1458–1463.
Kopec, R. E., Gleize, B., Borel, P., Desmarchelier, C., & Caris-Veyrat, C. (2017). Are lutein, lycopene, and β-carotene lost through the digestive process? *Food & Function, 8*, 1494–1503.
Krinsky, N. I., Landrum, J. T., & Bone, R. A. (2003). Biologic mechanisms of the protective role of lutein and zeaxanthin in the eye. *Annual Review of Nutrition, 23*, 171–201.
Kuang, P., Zhang, H., Bajaj, P. R., Yuan, Q., Tang, J., Chen, S., & Sablani, S. S. (2015). Physicochemical properties and storage stability of lutein microcapsules prepared with maltodextrins and sucrose by spray drying: physicochemical properties…. *Journal of Food Science, 80*(2), E359–E369.
Li, L. H., Lee, J. C.-Y., Leung, H. H., Lam, W. C., Fu, Z., & Lo, A. C. Y. (2020). Lutein supplementation for eye diseases. *Nutrients, 12*.
Lopez, C., Madec, M.-N., & Jimenez-Flores, R. (2010). Lipid rafts in the bovine milk fat globule membrane revealed by the lateral segregation of phospholipids and heterogeneous distribution of glycoproteins. *Food Chemistry, 120*(1), 22–33.
Lopez, C., Cheng, K., & Perez, J. (2018). Thermotropic phase behavior of milk sphingomyelin and role of cholesterol in the formation of the liquid ordered phase examined using SR-XRD and DSC. *Chemistry and Physics of Lipids, 215*, 46–55.
Ma, L.e., Dou, H.-L., Wu, Y.-Q., Huang, Y.-M., Huang, Y.-B., Xu, X.-R., Zou, Z.-Y., & Lin, X.-M. (2012). Lutein and zeaxanthin intake and the risk of age-related macular degeneration: A systematic review and meta-analysis. *British Journal of Nutrition, 107*(3), 350–359.
Makuch, K., Markiewicz, M., & Pasenkiewicz-Gierula, M. (2019). Asymmetric spontaneous intercalation of lutein into a phospholipid bilayer, a computational study. *Computational and Structural Biotechnology Journal, 17*, 516–526.
Mannock, D. A., McIntosh, T. J., Jiang, X., Covey, D. F., & McElhaney, R. N. (2003). Effects of natural and enantiomeric cholesterol on the thermotropic phase behavior and structure of egg sphingomyelin bilayer membranes. *Biophysical Journal, 84*(2), 1038–1046.
Mares, J. (2016). Lutein and zeaxanthin isomers in eye health and disease. *Annual Review of Nutrition, 36*(1), 571–602.
McIntosh, T. J. (1980). Differences in hydrocarbon chain tilt between hydrated phosphatidylethanolamine and phosphatidylcholine bilayers. A molecular packing model. *Biophysical Journal, 29*(2), 237–245.
Murillo, A. G., Aguilar, D., Norris, G. H., DiMarco, D. M., Missimer, A., Hu, S., Smyth, J. A., Gannon, S., Blesso, C. N., Luo, Y., & Fernandez, M. L. (2016). Compared with powdered lutein, a lutein nanoemulsion increases plasma and liver lutein, protects against hepatic steatosis, and affects lipoprotein metabolism in guinea pigs. *Journal of Nutrition, 146*(10), 1961–1969.
Pasenkiewicz-Gierula, M., Baczyński, K., Murzyn, K., & Markiewicz, M. (2012). Orientation of lutein in a lipid bilayer - revisited. *Acta Biochimica Polonica, 59*, 115–118.
Perry, A., Rasmussen, H., & Johnson, E. J. (2009). Xanthophyll (lutein, zeaxanthin) content in fruits, vegetables and corn and egg products. *Journal of Food Composition and Analysis, 22*(1), 9–15.
Ramstedt, B., & Slotte, J. P. (1999). Comparison of the biophysical properties of racemic and d-erythro-N-acyl sphingomyelins. *Biophysical Journal, 77*(3), 1498–1506.
Rasmussen, H. M., & Johnson, E. J. (2013). Nutrients for the aging eye.
Seddon, J. M., Ajani, U. A., Sperduto, R. D., Hiller, R., Blair, N., Burton, T. C., et al. (1994). Dietary carotenoids, vitamins A, C, and E, and advanced age-related macular degeneration. *JAMA, 272*, 1413–1420.
Shanmugam, S., Park, J.-H., Kim, K. S., Piao, Z. Z., Yong, C. S., Choi, H.-G., & Woo, J. S. (2011). Enhanced bioavailability and retinal accumulation of lutein from self-emulsifying phospholipid suspension (SEPS). *International Journal of Pharmaceutics, 412*(1-2), 99–105.
da Silva Santos, V., Badan Ribeiro, A. P., & Andrade Santana, M. H. (2019). Solid lipid nanoparticles as carriers for lipophilic compounds for applications in foods. *Food Research International, 122*, 610–626.
Simons, K., & Ikonen, E. (1997). Functional rafts in cell membranes. *Nature, 387*(6633), 569–572.
Singh, H. (2006). The milk fat globule membrane—A biophysical system for food applications. *Current Opinion in Colloid & Interface Science, 11*(2-3), 154–163.
Steiner, B. M., McClements, D. J., & Davidov-Pardo, G. (2018). Encapsulation systems for lutein: A review. *Trends in Food Science & Technology, 82*, 71–81.
Steiner, B. M., Shukla, V., McClements, D. J., Li, Y. O., Sancho-Madriz, M., & Davidov-Pardo, G. (2019). Encapsulation of lutein in nanoemulsions stabilized by resveratrol and maillard conjugates. *Journal of Food Science, 84*(9), 2421–2431.
Stelter, D., & Keyes, T. (2019). Simulation of fluid/gel phase equilibrium in lipid vesicles. *Soft Matter, 15*(40), 8102–8112.
Sujak, A., Okulski, W., & Gruszecki, W. I. (2000). Organisation of xanthophyll pigments lutein and zeaxanthin in lipid membranes formed with dipalmitoylphosphatidylcholine. *Biochimica et Biophysica Acta (BBA) - Biomembranes, 1509*(1-2), 255–263.
Swarnlata, S., D. G. (2011). Sphingosomes a novel approach to vesicular drug delivery.
Tan, C., Xia, S., Xue, J., Xie, J., Feng, B., & Zhang, X. (2013). Liposomes as vehicles for lutein: Preparation, stability, liposomal membrane dynamics, and structure. *Journal of Agriculture and Food Chemistry, 61*(34), 8175–8184.
Tardieu, A., Luzzati, V., & Reman, F. C. (1973). Structure and polymorphism of the hydrocarbon chains of lipids: A study of lecithin-water phases. *Journal of Molecular Biology, 75*(4), 711–733.
Thürmann, P. A., Schalch, W., Aebischer, J.-C., Tenter, U., & Cohn, W. (2005). Plasma kinetics of lutein, zeaxanthin, and 3-dehydro-lutein after multiple oral doses of a lutein supplement. *The American Journal of Clinical Nutrition, 82*, 88–97.
Vesper, H., Schmelz, E.-M., Nikolova-Karakashian, M. N., Dillehay, D. L., Lynch, D. V., & Merrill, A. H. (1999). Sphingolipids in food and the emerging importance of sphingolipids to nutrition. *Journal of Nutrition, 129*, 1239–1250.
Wu, J., Cho, E., Willett, W. C., Sastry, S. M., & Schaumberg, D. A. (2015). Intakes of lutein, zeaxanthin, and other carotenoids and age-related macular degeneration during 2 decades of prospective follow-up. *JAMA Ophthalmology, 133*(12), 1415.
Xia, F., Hu, D., Jin, H., Zhao, Y., & Liang, J. (2012). Preparation of lutein proliposomes by supercritical anti-solvent technique. *Food Hydrocolloids, 26*(2), 456–463.
Zaheer, K. (2017). Hen egg carotenoids (lutein and zeaxanthin) and nutritional impacts on human health: A review. *CyTA - Journal of Food, 15*(3), 474–487.
Zhao, L., Temelli, F., Curtis, J. M., & Chen, L. (2017). Encapsulation of lutein in liposomes using supercritical carbon dioxide. *Food Research International, 100*, 168–179.